

A bright, cold, velocity-controlled molecular beam by frequency-chirped laser slowing

S. Truppe,* H. Williams, M. Hambach, N. Fitch, T. E. Wall, E. A. Hinds, B. E. Sauer, and M. R. Tarbutt†
 Centre for Cold Matter, Blackett Laboratory, Imperial College London, Prince Consort Road, London SW7 2AZ UK
 (Dated: December 3, 2024)

Using frequency-chirped radiation pressure slowing we precisely control the velocity of a pulsed CaF molecular beam down to a few m/s, compressing its velocity spread by a factor of 10 while retaining its high brightness. When the final velocity is 15 m/s the flux, measured 1.3 m from the source, is 8×10^5 molecules per cm^2 per shot in a single rovibrational state. The beam is suitable for loading a magneto-optical trap of molecules. Our method, when combined with transverse laser cooling, can improve the precision of spectroscopic measurements that test fundamental physics. We compare the frequency-chirped slowing method with slowing using frequency-broadened light.

Great progress has recently been made on cooling molecules to ultracold temperatures, both by optoelectrical Sisyphus cooling [1–3] and direct laser cooling [4–13]. Following the initial demonstration of optical cycling in a beam of SrF [4], both Doppler cooling and Sisyphus cooling were used to reduce the transverse temperature of this beam [5]. It was shown that magneto-optical forces could be used to compress the transverse velocity distribution of a beam of YO [7], and then a three-dimensional magneto-optical trap (MOT) of SrF was demonstrated [9] and greatly improved [11, 12]. An important current challenge is to increase the number of molecules in the MOT by increasing the fraction delivered below the capture velocity, which is typically 10–20 m/s [14]. At present, radiation pressure slowing is used [6], with the spectral profile of the laser broadened to address a wide velocity range. This method has been applied to SrF [6], YO [10] and CaF [13], but typically slows the beam without compressing the velocity distribution, so only a small fraction of the initial distribution is delivered at the desired velocity.

Molecular beams are increasingly being used for precise measurements that test fundamental physics. This includes measurements of the electron’s electric dipole moment [15, 16], measurements of parity violation in nuclei [17] and chiral molecules [18], and searches for hypothesized changes to the fundamental constants [19–21]. These are spectroscopic measurements whose precision scales linearly with the time each molecule spends in the experiment, and so they could be greatly improved using colder and slower beams. A centrifuge decelerator [22] has been used to slow continuous beams to low velocity, while Stark deceleration [23], and its variants [24–26], produce velocity-controlled pulsed beams. These typically accept only a small fraction of the initial velocity distribution, do not provide cooling, and become difficult, though not impossible [27], to implement for heavy molecules. Here, we use frequency-chirped laser slowing to compress the entire velocity distribution of a beam of CaF into a narrow range and slow the beam to the desired final velocity.

Figure 1 shows the relevant energy levels of CaF and the vibrational branching ratios between them. Rota-

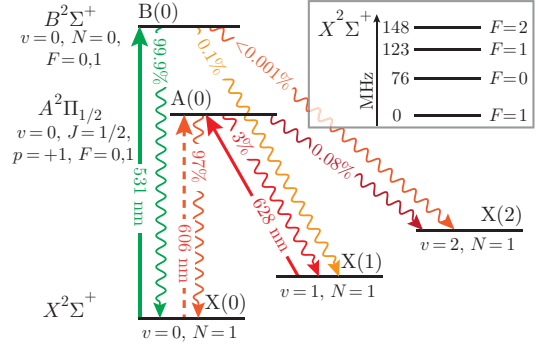


FIG. 1. Relevant energy levels of CaF, with calculated vibrational branching ratios [28, 29], and the transitions used for slowing (solid lines) and detection (dashed line). Wavy lines are spontaneous decays. v is the vibrational quantum number, p the parity, and N, J , and F the rotational, total electronic and total angular momentum quantum numbers respectively. We use $X(v)$, $A(v)$ and $B(v)$ to denote the states shown. Inset: hyperfine structure in $X(0)$ [30]. The hyperfine interval of $B(0)$ is 20(5) MHz and of $A(0)$ is < 10 MHz [14].

tional branching is forbidden by the electric dipole selection rules [5, 31]. The main cooling transition is $B(0)\text{--}X(0)^1$ with wavelength $\lambda_{\text{main}} = 531$ nm, linewidth $\Gamma = 2\pi \times 6.3$ MHz [32] and single-photon recoil velocity 0.013 m/s. Population that leaks into $X(1)$ is returned to the cooling cycle via the $A(0)\text{--}X(1)$ transition at $\lambda_{\text{repump}} = 628$ nm. The branching ratios on the $B\text{--}X$ transition are so favourable that only these two laser wavelengths are needed to bring a buffer-gas cooled molecular beam to rest by scattering > 10000 photons per molecule. Because the two transitions have different upper states, the scattering rate is increased by almost a factor of 2 compared to previous work on laser cooling of molecules where $X(0)$ and $X(1)$ were both driven to $A(0)$. This is because, when N_g ground states are all coupled to a single excited state, the maximum scattering rate is $\Gamma/(N_g + 1)$ [33].

Figure 2(a) illustrates the experiment. A pulsed beam

¹ See Fig. 1 for the notation used throughout this paper

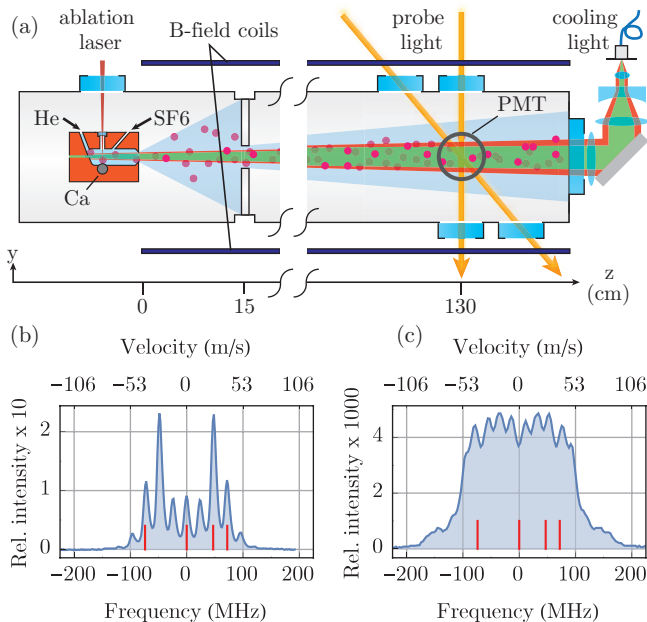


FIG. 2. (a) Apparatus. A pulsed beam of CaF from a cryogenic source is slowed by a counter-propagating laser beam. Molecules are detected by LIF at $z = 130$ cm, using a probe laser propagating at either 90° or 60° to the molecular beam. (b,c) Spectrum of main cooling laser for experiments with (b) frequency-chirped light, and (c) frequency-broadened light, both measured by a spectrum analyzer with 10 MHz linewidth. Lines mark frequencies of hyperfine components.

of CaF is produced by a cryogenic buffer gas source [34–36]. At $t = 0$, a pulsed laser (5 mJ, 4 ns, 1064 nm) ablates Ca into a 4 K copper cell, through which flow 1 sccm of 4 K helium and 0.01 sccm of 270 K SF₆. The Ca reacts with the SF₆ to form CaF molecules, which are then cooled by the He and entrained in the flow. The molecules exit the cell at $z = 0$ through a 3.5 mm diameter aperture, and are collimated by an 8 mm diameter aperture at $z = 15$ cm which separates the source from the main chamber, where the pressure is 3×10^{-7} mbar. The average flux is 1.6×10^{11} CaF molecules per steradian per shot in $X(0)$, and the pulse duration measured at $z = 2.5$ cm is $280 \mu\text{s}$ (FWHM). At $z = 130$ cm the molecules are detected by driving the $A(0) \leftarrow X(0)$ transition at 606 nm, imaging the resulting laser-induced fluorescence (LIF) onto a photomultiplier tube (PMT), and recording the signal with a time resolution of $5 \mu\text{s}$, yielding a time-of-flight (ToF) profile. The probe laser has a gaussian intensity distribution with a $1/e^2$ diameter of 6 mm and a power of 5 mW, and it crosses the molecular beam at 90° for velocity-insensitive measurements, or 60° for velocity-sensitive measurements. Molecules which pass through the $\approx 0.3 \text{ cm}^2$ area of the detector are detected. We add rf sidebands to the probe beam, using a 72 MHz electro-optic modulator (EOM) and a 48 MHz acousto-optic modulator (AOM), so that all four hyperfine com-

ponents of the transition are addressed (Fig. 1,[8]).

The cooling light is collimated, has a gaussian intensity distribution with a $1/e^2$ diameter of 6 mm, counter-propagates to the molecular beam, and consists of 110 mW at λ_{main} , which is applied for times between t_{start} and t_{end} , and 100 mW at λ_{repump} which is applied continuously. The two wavelengths have orthogonal linear polarizations, both at 45° to a uniform 0.5 mT magnetic field directed along y which prevents optical pumping into dark Zeeman sub-levels [4, 31, 37]. A mechanical shutter blocks the main cooling light on alternate shots of the source to control against source fluctuations. The frequencies of all lasers are stabilized to a 780 nm laser, itself locked to a saturated absorption feature of Rb, via a scanning transfer cavity. We find the frequency that maximizes the LIF when the main cooling laser is used as an orthogonal probe, then lock its frequency at this value. We do the same for the repump laser. Using the transfer cavity as a calibrated frequency reference, we detune both lasers so that, when counter-propagating to the molecules, they are resonant with those travelling with speed v_{start} . To account for the changing Doppler shift as the molecules slow down, we apply linear frequency chirps to the main and repump lasers, with chirp rates β and $\beta\lambda_{\text{main}}/\lambda_{\text{repump}}$ respectively. At the end of the cooling period, the light is resonant with molecules travelling at speed $v_{\text{end}} = v_{\text{start}} - \beta\lambda_{\text{main}}(t_{\text{end}} - t_{\text{start}})$. To address all the hyperfine components, we generate the laser spectrum shown in Fig. 2(b) by passing both lasers through EOMs driven at 24 MHz with a phase modulation index of 3.1. We compare this frequency-chirp method to the frequency-broadened method used in previous work [6, 10, 13]. Here, we fix the frequencies but spectrally broaden the light to address a wide range of velocities. This is achieved by sending the light through three consecutive EOMs driven at 72, 24, and 8 MHz, producing the spectrum shown in Fig. 2(c).

Figure 3 shows typical cooling data and illustrates our analysis method. We refer to data with the cooling light off and on as “control” and “cooled” respectively. Figure 3(a) shows the control and cooled ToF profiles recorded using the 90° probe, each averaged over 50 shots. The cooling light depletes the ToF profile between 6 and 13 ms, but enhances the number arriving at later times. To measure the velocity profile we first record a Doppler-free reference spectrum using the 90° probe. The peak fluorescence signal in this spectrum defines the zero of frequency. We then measure a Doppler broadened spectrum using the 60° probe. We partition this data by arrival time, typically using 0.5 ms-wide time windows. Within such a narrow time window, the range of velocities is small, so the spectrum is similar to the reference spectrum, but shifted according to the mean velocity. Figure 3(b) shows the control and cooled spectra for molecules arriving between 7.5 and 8 ms. Because there are four hyperfine components, and the light has

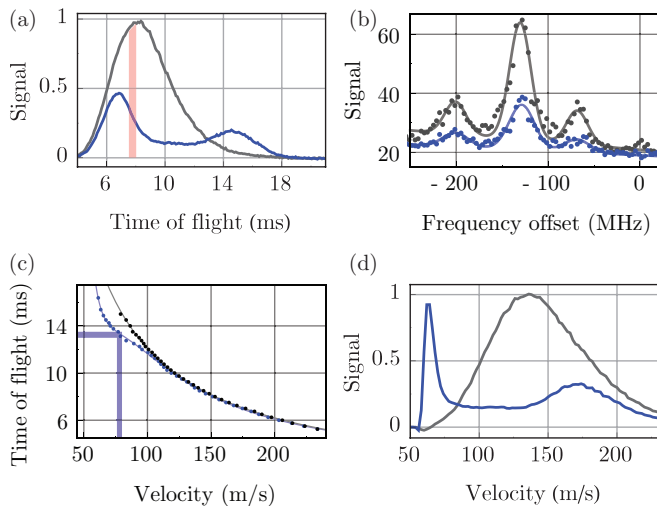


FIG. 3. Slowing and cooling using $\beta = 21$ MHz/ms, $t_{\text{start}} = 1$ ms, $t_{\text{end}} = 7$ ms, $v_{\text{start}} = 178$ m/s. Throughout, blue and grey data have cooling light on and off respectively. (a) ToF profiles. (b) Spectrum recorded using 60° probe, for molecules arriving in the 7.5–8 ms time window [vertical band in (a)]. The Doppler shift determines their velocity. Dots: data. Lines: fit to sum of three gaussians. (c) Dots: mean arrival time versus velocity determined this way. Lines: fits (see main text). From these curves, and the ToF profiles in (a), we determine (d) the velocity profiles.

multiple rf sidebands, there are several peaks in the spectrum, three of which are clear in the data. The largest peak is obtained when all 4 hyperfine components are simultaneously resonant. We fit the data to a sum of three gaussians and use the fitted centre frequency of the largest peak to determine the mean velocity. Applying this procedure to all time windows gives graphs of arrival time versus velocity, as in Fig. 3(c). We generate smooth curves to represent the data, shown by solid lines, by fitting the model $t = \sum_{n=0}^m a_n/v^n$ with a_n as free parameters. The control data fits well with $m = 1$, as we would expect when there is no deceleration. For the cooled data, we take $m = 5$. We see that at high velocities, the relation between velocity and arrival time is independent of whether or not the cooling light is on, but at low speeds they differ. The molecules that arrive after 12 ms travel more slowly when the cooling light is on, and the curve acquires a much steeper gradient at low velocity. Molecules arriving in a wide time window from 14 to 17 ms all have speeds between 60 and 70 m/s. To find the number of molecules with velocity v , we use the curves of Fig. 3(c) to find the times t_1, t_2 corresponding to $v + \Delta v$ and $v - \Delta v$ with $\Delta v = 2$ m/s, then integrate the ToF profile between t_1 and t_2 . Doing this for all velocities gives the control and cooled velocity distributions shown in Fig. 3(d). In the cooled data, a large fraction of the molecules are slowed into a narrow bunch centred at 63 m/s. The width of this peak corresponds to a temper-

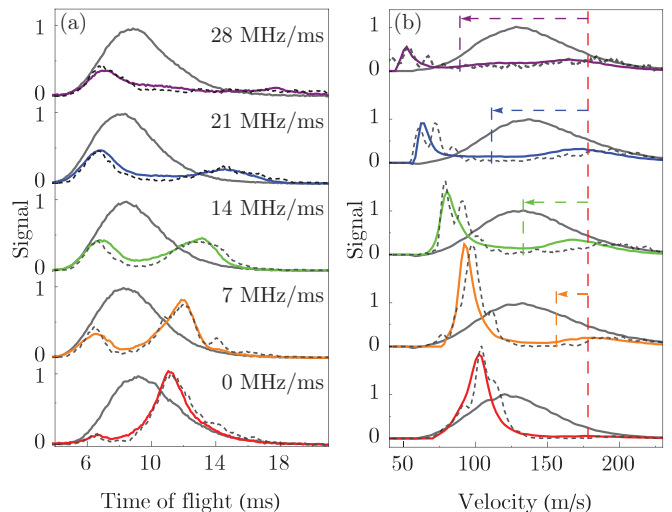


FIG. 4. Laser slowing for various chirp rates, β . Other parameters are $t_{\text{start}} = 1$ ms, $t_{\text{end}} = 7$ ms, $v_{\text{start}} = 178$ m/s. (a) ToF profiles and (b) velocity distributions, with cooling off (solid grey) and on (solid coloured). Black dashed curves overlaid with experimental data are simulation results. Vertical dashed lines in (b) indicate v_{start} (red) and v_{end} (other colours).

ature of 100 mK, limited by the velocity resolution of the measurement. The reduction in the number of detected molecules is due to the increased divergence of the slowed beam, resulting in fewer molecules passing through the detection volume. This has been observed previously [6], and is discussed further below.

The solid curves in Fig. 4 are experimental control and cooled ToF profiles and velocity distributions for various chirp rates, with $t_{\text{start}} = 1$ ms, $t_{\text{end}} = 7$ ms, and $v_{\text{start}} = 178$ m/s. Even with no chirp, the molecules are slowed to about 100 m/s and their velocity distribution is compressed. As β increases, the molecules are pushed to lower velocities, and while they arrive at the detector over a broad range of times, they always have a narrow velocity distribution. The final velocity is always lower than v_{end} , indicating that the molecules follow the changing frequency up to the highest β used. The dashed curves in Fig. 4 are simulation results. For each simulation, we use a rate model [38] to determine the scattering rate as a function of detuning and power, and then calculate the resulting trajectories of many molecules using the experimental parameters and measured initial velocity distributions as inputs. The randomness of the momentum kicks is included. The simulations show some structure in the slowed peak that is not observed experimentally, but all other features agree well. For all β , the simulations accurately predict the observed ToF profiles and velocity distributions, including the overall loss of detected molecules, the amplitudes and widths of the distribution of slowed molecules, and the amplitude and shape of the distribution of faster molecules left behind by the chirp.

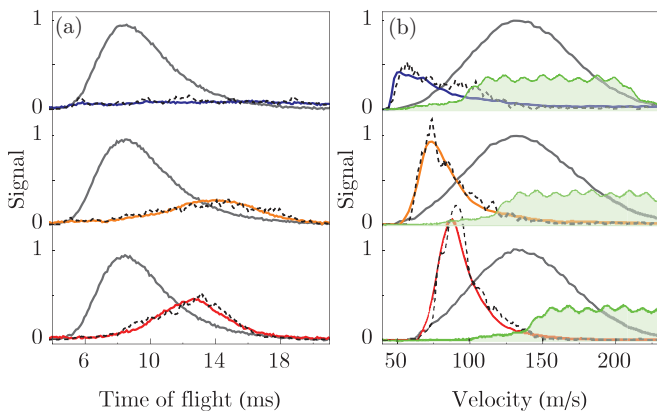


FIG. 5. Laser slowing using frequency-broadened light. Parameters are $t_{\text{start}} = 1$ ms, $t_{\text{end}} = 7$ ms, $\beta = 0$. (a) ToF profiles and (b) velocity distributions, with cooling off (solid grey) and on (solid coloured). Black dashed curves overlaid with experimental data are simulation results. Shaded area in (b): spectrum of light used in each case.

This shows that the photon scattering rate is as expected and that the experiment is very well understood.

Figure 5 shows ToF profiles and velocity distributions measured when we use frequency-broadened light with no chirp. Again, we see that we address most of the molecules and slow them efficiently. By changing the central frequency of the light, we control the final velocity. The velocity distribution is not as narrow as in the chirp data, but it is compressed. This is expected [39] because the velocity dependence of the force reflects the roughly top-hat spectral profile of the light, and so all molecules tend to be slowed until their Doppler shift is slightly below the low frequency cut-off of the broadened laser spectrum. Again, the simulations agree very well with the measured ToF profiles and velocity distributions, showing that this case is also well understood.

In both the frequency-chirped and frequency-broadened experiments the cooling light has no effect on the measured ToF profile when no magnetic field is applied. As the field is increased the deceleration increases until the field is 0.5 mT where the effect saturates. Switching the polarization of the light [7, 37] at 5 MHz, with no applied magnetic field, gives exactly the same results as a static polarization and a 0.5 mT magnetic field. In the frequency-chirped experiments the deceleration saturates at an on-axis laser intensity of ≈ 350 mW/cm², and in the frequency-broadened experiments it saturates at ≈ 750 mW/cm².

Both slowing techniques show a decrease in the number of detected molecules the further we slow them. The vast majority of the loss is due to the increased divergence of the slower molecules, which, after t_{end} , drift freely for up to 10 ms before reaching the detector. The excellent agreement between experiment and simulation confirms this, since there are no other loss mechanisms

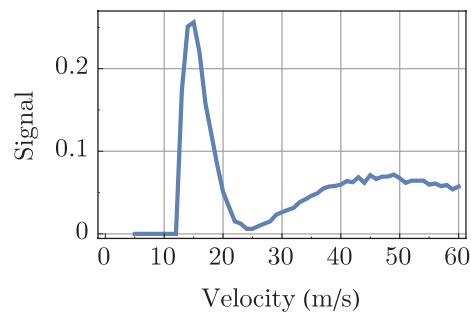


FIG. 6. Velocity distribution for $t_{\text{start}} = 3.5$ ms, $t_{\text{chirp}} = 4$ ms, $t_{\text{end}} = 12$ ms, $\beta = 37$ MHz/ms, $v_{\text{start}} = 178$ m/s, and a converging laser beam. The scaling is the same as in Fig. 4, i.e. the control distribution has an amplitude of 1.

in the simulations. According to the simulations, when $\beta = 21$ MHz/ms transverse heating accounts for only 8% of the total loss in detected molecules. We have investigated all potential loss channels that might take population out of the cooling cycle. To determine the fraction that leaks to state q , we scan the probe laser over a transition from q and measure the increase in fluorescence signal when the cooling light is applied with the same parameters as in the $\beta = 21$ MHz/ms data in Fig. 4. We determine the fraction $f(q) = \Delta P(q)/P_0$ where P_0 is the initial population in $X(0)$ and $\Delta P(q)$ is the change in the population of q . We measured the leak to $v = 2$ by scanning $A(2) \leftarrow X(2)$ and find $f(v = 2) = 3.7(1)\%$. The simulations reproduce this result when we set the $B(0) \leftarrow X(2)$ branching ratio to 0.0015(3)%. We measure the loss to the even parity $N = 0$ and $N = 2$ states of X , which are not part of the cooling cycle, by scanning over the $Q(0)$ and $Q(2)$ lines of the $A^2\Pi_{1/2}(v = 0) \leftarrow X^2\Sigma^+(v = 0)$ transition, and find $f(N = 0) = 1.6(2)\%$ and $f(N = 2) = 0.4(2)\%$ corresponding to branching ratios of 0.0007(1)% and 0.00016(3)% respectively. The most obvious route to these states is the decay chain $B \rightarrow A \rightarrow X$, though there are other possibilities, including magnetic dipole transitions which are sometimes surprisingly intense in molecules [40]. With similar sensitivity, we searched for possible loss to $N = 3$ induced by a term in the hyperfine Hamiltonian that couples states with $\Delta N = 2$, but found nothing. From all these measurements we conclude that ~ 30000 photons per molecule can be scattered before half the molecules are lost from the cooling cycle.

We increase the number of detected molecules in three ways. First, we add a small transverse force by focusing the cooling light so that it converges with an angle of 8.2 mrad to a $1/e^2$ diameter of 3 mm at $z = 0$. Using the same parameters as the $\beta = 21$ MHz/ms data in Fig. 4, we find that the converging light beam increases the number of detected molecules by 60% relative to the collimated beam of the same power. Second, we reduce the free flight time for slowed molecules by shifting t_{end}

closer to the time when they are detected. This complicates the interpretation of the ToF profile, because the faster molecules arrive when the cooling light is still on, but makes it easier to detect the slower ones because more reach the detector. Third, we change the chirp ramp so that the frequency is constant between t_{start} and t_{chirp} , then linearly chirped between t_{chirp} and t_{end} . This pushes the faster molecules to lower velocities before the chirp begins, so that they are no longer left behind, and increases the number of detected slow molecules by about 50% when $t_{\text{chirp}} - t_{\text{start}} = 1$ ms. Figure 6 shows the velocity distribution measured with these improvements. The molecules are slowed to 15 m/s and the flux is $(8_{-2}^{+4}) \times 10^5$ molecules per cm^2 per pulse in a velocity interval of 15 ± 5 m/s. This velocity is below the predicted capture velocity of a CaF MOT [14] with $1/e^2$ beam sizes of 12 mm and readily available powers. Thus we expect 10^5 – 10^6 molecules per pulse to be within both the capture volume and capture velocity of a MOT. Given the increase in flux we already observe when using a converging cooling beam, we believe the flux could be greatly increased using a short region of transverse laser cooling near the source. Combining transverse cooling [5] with this longitudinal laser slowing and cooling method would produce an intense, collimated, slow and velocity-controlled beam with the potential to improve the precision of measurements that test fundamental physics.

The research leading to these results has received funding from EPSRC under grants EP/I012044 and EP/M027716, and from the European Research Council under the European Union’s Seventh Framework Programme (FP7/2007-2013) / ERC grant agreement 320789.

* s.truppe09@imperial.ac.uk

† m.tarbutt@imperial.ac.uk

- [1] M. Zeppenfeld, M. Motsch, P. W. H. Pinkse, and G. Rempe, *Phys. Rev. A* **80**, 041401 (2009).
- [2] M. Zeppenfeld, B. G. U. Englert, R. Glöckner, A. Prehn, M. Mielenz, C. Sommer, L. D. van Buuren, M. Motsch, and G. Rempe, *Nature* **491**, 570 (2012).
- [3] A. Prehn, M. Ibrügger, R. Glöckner, G. Rempe, and M. Zeppenfeld, *Phys. Rev. Lett.* **116**, 063005 (2016).
- [4] E. S. Shuman, J. F. Barry, D. R. Glenn, and D. DeMille, *Phys. Rev. Lett.* **103**, 1 (2009).
- [5] E. S. Shuman, J. F. Barry, and D. DeMille, *Nature* **467**, 820 (2010).
- [6] J. F. Barry, E. S. Shuman, E. B. Norrgard, and D. DeMille, *Phys. Rev. Lett.* **108**, 103002 (2012).
- [7] M. T. Hummon, M. Yeo, B. K. Stuhl, A. L. Collopy, Y. Xia, and J. Ye, *Phys. Rev. Lett.* **110**, 143001 (2013).
- [8] V. Zhelyazkova, A. Cournol, T. E. Wall, A. Matsushima, J. J. Hudson, E. A. Hinds, M. R. Tarbutt, and B. E. Sauer, *Phys. Rev. A* **89**, 053416 (2014).
- [9] J. F. Barry, D. J. McCarron, E. B. Norrgard, M. H. Steinecker, and D. DeMille, *Nature* **512**, 286 (2014).
- [10] M. Yeo, M. T. Hummon, A. L. Collopy, B. Yan, B. Hemmerling, E. Chae, J. M. Doyle, and J. Ye, *Phys. Rev. Lett.* **114**, 223003 (2015).
- [11] D. J. McCarron, E. B. Norrgard, M. H. Steinecker, and D. DeMille, *New J. Phys.* **17**, 035014 (2015).
- [12] E. B. Norrgard, D. J. McCarron, M. H. Steinecker, M. R. Tarbutt, and D. DeMille, *Phys. Rev. Lett.* **116**, 063004 (2016).
- [13] B. Hemmerling, E. Chae, A. Ravi, L. Anderegg, G. K. Drayna, N. R. Hutzler, A. L. Collopy, J. Ye, W. Ketterle, and J. M. Doyle, arXiv:1603.02787.
- [14] M. R. Tarbutt and T. C. Steimle, *Phys. Rev. A* **92**, 053401 (2015).
- [15] J. J. Hudson, D. M. Kara, I. J. Smallman, B. E. Sauer, M. R. Tarbutt, and E. A. Hinds, *Nature* **473**, 493 (2011).
- [16] J. Baron, W. C. Campbell, D. DeMille, J. M. Doyle, G. Gabrielse, Y. V. Gurevich, P. W. Hess, N. R. Hutzler, E. Kirilov, I. Kozryyev, B. R. O’Leary, C. D. Panda, M. F. Parsons, E. S. Petrik, B. Spaun, A. C. Vutha, and A. D. West, *Science* **343**, 269 (2014).
- [17] S. B. Cahn, J. Ammon, E. Kirilov, Y. V. Gurevich, D. Murphree, R. Paolino, D. A. Rahmlow, M. Kozlov, and D. DeMille, *Phys. Rev. Lett.* **112**, 163002 (2014).
- [18] C. Daussy, T. Marrel, A. Amy-Klein, C. T. Nguyen, C. J. Bordé, and C. Chardonnet, *Phys. Rev. Lett.* **83**, 1554 (1999).
- [19] A. Shelkownikov, R. J. Butcher, C. Chardonnet, and A. Amy-Klein, *Phys. Rev. Lett.* **100**, 150801 (1999).
- [20] E. R. Hudson, H. J. Lewandowski, B. C. Sawyer, and J. Ye, *Phys. Rev. Lett.* **96**, 143004 (2006).
- [21] S. Truppe, R. J. Hendricks, S. K. Tokunaga, H. J. Lewandowski, M. G. Kozlov, C. Henkel, E. A. Hinds, and M. R. Tarbutt, *Nat. Commun.* **4**, 2600 (2013).
- [22] S. Chervenkov, X. Wu, J. Bayerl, A. Rohlfes, T. Gantner, M. Zeppenfeld, and G. Rempe, *Phys. Rev. Lett.* **112**, 013001 (2014).
- [23] H. L. Bethlem, G. Berden, and G. Meijer, *Phys. Rev. Lett.* **83**, 1558 (1999).
- [24] A. Osterwalder, S. A. Meek, G. Hammer, H. Haak, and G. Meijer, *Phys. Rev. A* **81**, 051401(R) (2010).
- [25] R. Fulton, A. I. Bishop, and P. R. Barker, *Phys. Rev. Lett.* **93**, 243004 (2004).
- [26] E. Narevicius, A. Libson, C. Parthey, I. Chavez, J. Narevicius, U. Even, and M. G. Raizen, *Phys. Rev. A* **77**, 051401 (2008).
- [27] J. van den Berg, S. Mathavan, C. Meinema, J. Nauta, T. Nijbroek, K. Jungmann, H. Bethlem, and S. Hoekstra, *J. Mol. Spectrosc.* **300**, 22 (2014).
- [28] M. Pelegrini, C. S. Vivacqua, O. Roberto-Neto, F. R. Ornellas, and F. B. C. Machado, *Braz. J. Phys.* **35**, 950 (2005).
- [29] M. Dulick, P. F. Bernath, and R. W. Field, *Can. J. Phys.* **58**, 703 (1980).
- [30] W. Childs, G. L. Goodman, and L. S. Goodman, *J. Mol. Spectrosc.* **86**, 365 (1981).
- [31] B. K. Stuhl, B. C. Sawyer, D. Wang, and J. Ye, *Phys. Rev. Lett.* **101**, 243002 (2008).
- [32] P. J. Dagdigian, H. W. Cruse, and R. N. Zare, *J. Chem. Phys.* **60**, 2330 (1974).
- [33] M. R. Tarbutt, B. E. Sauer, J. J. Hudson, and E. A. Hinds, *New J. Phys.* **15**, 053034 (2013).
- [34] N. R. Hutzler, H.-I. Lu, and J. M. Doyle, *Chem. Rev.* **112**, 4803 (2012).
- [35] J. F. Barry, E. S. Shuman, and D. DeMille,

- Phys. Chem. Chem. Phys. **13**, 18936 (2011).
- [36] N. E. Bulleid, S. M. Skoff, R. J. Hendricks, B. E. Sauer, E. A. Hinds, and M. R. Tarbutt, Phys. Chem. Chem. Phys. **15**, 12299 (2013).
- [37] D. J. Berkeland and M. G. Boshier, Phys. Rev. A **65**, 033413 (2002).
- [38] M. R. Tarbutt, New J. Phys. **17**, 015007 (2015).
- [39] M. Zhu, C. W. Oates, and J. L. Hall, Phys. Rev. Lett. **67**, 46 (1991).
- [40] M. Kirste, X. Wang, G. Meijer, K. B. Gubbels, A. van der Avoird, G. C. Groenenboom, and S. Y. T. van de Meerakker, J. Chem. Phys. **137**, 101102 (2012).